Current Biology 22, 2278–2283, December 4, 2012 ©2012 Elsevier Ltd All rights reserved http://dx.doi.org/10.1016/j.cub.2012.10.019

Report

oskar Predates the Evolution of Germ Plasm in Insects

Ben Ewen-Campen,[1] John R. Srouji,[2] Evelyn E. Schwager,[1] and Cassandra G. Extavour[1,*]
[1]Department of Organismic and Evolutionary Biology
[2]Department of Molecular and Cellular Biology
Harvard University, 16 Divinity Avenue, Cambridge, MA 02138, USA

Summary

***oskar* is the only gene in the animal kingdom necessary and sufficient for specifying functional germ cells [1, 2]. However, *oskar* has only been identified in holometabolous ("higher") insects that specify their germline using specialized cytoplasm called germ plasm [3]. Here we show that *oskar* evolved before the divergence of higher insects and provide evidence that its germline role is a recent evolutionary innovation. We identify an *oskar* ortholog in a basally branching insect, the cricket *Gryllus bimaculatus*. In contrast to *Drosophila oskar*, *Gb-oskar* is not required for germ cell formation or axial patterning. Instead, *Gb-oskar* is expressed in neuroblasts of the brain and CNS and is required for neural development. Taken together with reports of a neural role for *Drosophila oskar* [4], our data demonstrate that *oskar* arose nearly 50 million years earlier in insect evolution than previously thought, where it may have played an ancestral neural role, and was co-opted to its well-known essential germline role in holometabolous insects.**

Results and Discussion

Animal germ cells can be specified either through the cytoplasmic inheritance of maternally deposited germ plasm or through inductive cell signaling [5]. In *Drosophila melanogaster*, germ cells form by incorporating germ plasm deposited and localized at the oocyte posterior. Germ plasm assembly requires *oskar* [6], which is necessary and sufficient for germ cell specification [1, 2]. Oskar is localized at the oocyte posterior, where it promotes the accumulation of conserved germline factors including Vasa, PIWI, and Tudor proteins [7] and induces posterior patterning by recruiting *nanos* mRNA [8]. Despite its essential role in *Drosophila* germ cell formation and axial patterning, *oskar* has only been identified in the genomes of a small number of holometabolous insects, all of which specify their germ cells via germ plasm [3]. In contrast, *oskar* is absent from the genomes of holometabolous insects that lack germ plasm, and neither *oskar* nor germ plasm have been identified in any insect taxa that branch basally to Holometabola [3]. The prevailing hypothesis is therefore that *oskar* arose as a novel gene at the base of Holometabola coincidentally with the evolution of insect germ plasm [3].

Here we report the first discovery of an *oskar* ortholog in a basally branching insect that lacks germ plasm, the cricket *Gryllus bimaculatus* (Orthoptera). We unexpectedly detected *Gb-oskar* in a combined *Gryllus* ovarian and embryonic de novo transcriptome. Three lines of evidence confirm that *Gb-oskar* is a bona fide *oskar* ortholog. First, Gb-Oskar is the reciprocal best protein BLAST hit against the protein products of all known *oskar* genes from flies, mosquitoes, ants, and the wasp *Nasonia*. Second, *Gb-oskar* encodes the LOTUS (aka OST-HTH) and SGNH hydrolase domains that characterize all *oskar* orthologs [3, 9, 10] (Figures 1A and see Figure S1 available online). Physicochemical conservation is pronounced within both the LOTUS and SGNH hydrolase domains of Gb-Oskar (37.1% and 36.3%, respectively), while amino acid identity is less strongly conserved (11.4% and 21.2%, respectively), consistent with previous observations of *oskar* orthologs [3, 11]. Third, phylogenetic reconstruction clearly places *Gb-oskar* with other known *oskar* genes and not within the *tdrd7* genes (Figure 1B), a conserved metazoan gene family that also contains the LOTUS domain [9, 10]. Thus, in contrast to previous hypotheses that *oskar* first arose in the lineage leading to the Holometabola [3], our analyses demonstrate that *oskar* was present at least ~50 million years earlier than previously thought [3] in the common ancestor of Orthoptera and Holometabola [12].

The presence of *oskar* in the genome of an insect branching basal to the Holometabola is surprising because neither germ plasm nor pole cells have been described in any of these taxa. Instead, germ cells are thought to arise from the mesoderm during midembryogenesis in orthopterans [13] and most other early diverging insects [14]. We therefore asked whether *Gb-oskar* plays a conserved role in germ cell formation in *Gryllus* or whether this function arose later during insect evolution. We examined the expression of *Gb-oskar* mRNA and protein (Figure S2) during oogenesis and embryogenesis. In stark contrast to *oskar* expression in *Drosophila* [15] and *Nasonia* [3], *Gb-oskar* mRNA and protein do not accumulate at the posterior of *Gryllus* oocytes and instead are distributed ubiquitously throughout all stages of oogenesis (Figures 2A–2D). In just-laid eggs, *Gb-oskar* mRNA does not localize posteriorly and is barely detectable by in situ hybridization (Figure 2E), although RT-PCR confirms that *Gb-oskar* is expressed throughout all stages of embryogenesis (Figure 2J). *Gryllus* primordial germ cells, marked by *Gb-piwi* and *Gb-vasa* transcript (Figures 2H and 2I) and protein (Figures 2H′ and 2I′; Figures S2G and S2H) expression, arise during abdominal segmentation stages, but expression of both *Gb-oskar* mRNA and Gb-Oskar protein remains at low levels in all embryonic cells throughout these stages and does not become enriched in primordial germ cells before or during their formation (Figures 2G and 2G′). The expression pattern of *Gb-oskar* therefore does not support a role for this gene in germ cell formation.

To directly test whether *Gb-oskar* is functionally required for germ cell formation in *Gryllus*, we knocked down *Gb-oskar* function during oogenesis and embryogenesis using maternal RNAi (mRNAi) and embryonic RNAi (eRNAi), respectively [16] (Figures 2, S3A, and S3B). In contrast to *Drosophila* and *Nasonia*, maternal knockdown of *Gb-oskar* did not reduce egg laying (Figure S3C), affect ovary morphology, or impede

*Correspondence: extavour@oeb.harvard.edu

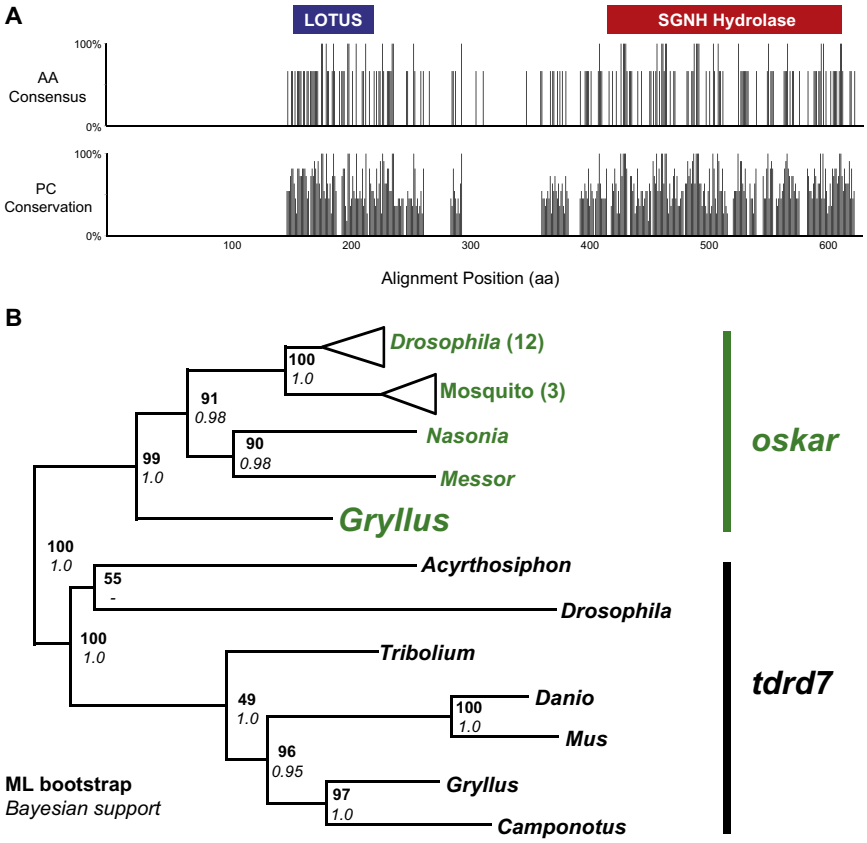

Figure 1. Domain Structure and Phylogenetic Analysis of *Gb-oskar*

(A) ClustalW protein alignment of Oskar orthologs from *Gryllus bimaculatus*, *Nasonia vitripennis*, and *Drosophila melanogaster* (see Figure S1 for alignment showing amino acids). Sequence identity at the amino acid level is not strongly conserved (top graph), but physicochemical conservation is more pronounced (bottom graph), specifically within the conserved LOTUS (blue) and SGNH hydrolase (red) domains in all three proteins, meaning that the chemical properties of these domains are conserved at a local level despite amino acid divergence and suggesting that these regions may represent functional domains of Oskar. (B) Phylogenetic reconstruction of *Gb-oskar* with known *oskar* (green) and *tdrd7* (black) orthologs. The best-scoring unrooted ML topology is shown: bold, ML bootstrap values; italics, Bayesian posterior probability.

the progress of oogenesis (Figure S3D). Embryonic *Gb-oskar* knockdown did not cause any of the posterior patterning defects seen in *Drosophila osk* mutants [6] (Figure S3E, Table S1), and these embryos were morphologically wild-type and hatched at normal rates (Figure S3F). These data show that in contrast to the known requirement for *oskar* in anterior-posterior (A-P) axial patterning in holometabolous insects [3, 6], *oskar* does not direct *Gryllus* axial patterning. Further, *Gb-oskar* eRNAi embryos produced germ cells that expressed Gb-Piwi and Gb-Vasa (Figures 2K–2N) and ultimately produced functional ovaries in adulthood (Figure 2P).

In contrast to the essential and conserved role that *oskar* plays in Holometabolous germ cell formation [3, 8], our analyses of *Gb-oskar* gene expression and function show that this gene is not required for germ cell formation in *Gryllus*. We therefore hypothesized that *Gb-oskar* has a distinct somatic function in *Gryllus* that may reflect an ancestral function for this gene. Consistent with this hypothesis, we observed that *Gb-oskar* has a specific somatic expression pattern during midembryogenesis: *Gb-oskar* mRNA and protein are enriched in neuroblasts along the A-P axis (Figures 3A–3C″). Neuroblasts are neural stem cells that arise from the ventral ectoderm and produce neurons of the CNS in *Drosophila* and other Pancrustacea (insects and crustaceans) [17]. *Gb-oskar* expression in the neuroblasts begins during the earliest stages of neurogenesis and persists throughout all stages examined. In addition to this embryonic expression pattern, *Gb-oskar* is also expressed in the adult brain (Figure 2J).

We examined embryonic nervous system development in *Gb-oskar* knockdown conditions and found that *Gb-oskar* eRNAi embryos exhibit morphological defects of the axonal tracts that are consistent with an impairment of neuroblast divisions: lateral connectives are often broken or reduced in width compared to controls (Figures 3D–3D″, $p < 0.001$), anterior commissure formation is significantly delayed or absent (Figures 3E–3E″, $p < 0.01$), and posterior commissure formation is similarly disrupted (Figures 3F–3F″, $p < 0.025$). These axonal defects suggest that *Gb-oskar* may be required for proper neuronal determination and are reminiscent of the axonal scaffold defects of *Drosophila miranda* and *prospero* mutants, which disrupt neuroblast divisions resulting in neuronal misspecification [18].

Aberrant neuroblast divisions can be assayed by examining the expression of *even-skipped*, which is expressed in a stereotyped subset of ganglion mother cells and neurons within each segment, including the aCC and pCC neurons that are homologous across insects [19]. We found that 34.5% of *Gb-oskar* eRNAi embryos displayed significant defects in aCC/pCC specification (Figures 3G–3G″, $p < 0.01$) that were never observed in controls, indicating that *Gb-oskar* is required for proper neuroblast division.

Our results demonstrate a role for *Gb-oskar* in the development of the cricket CNS, in contrast to its well-known role in germ plasm formation in holometabolous insects. These divergent functions of *oskar* suggest at least two possible evolutionary scenarios. First, *oskar*'s ancestral role in insects could be that of germ plasm assembly as seen in *Drosophila*, and the CNS function we report here could be a derived trait in the branch of the insect tree leading to *Gryllus*. However, several lines of evidence support a second scenario, whereby *oskar*'s neural function is ancestral to Orthoptera (crickets, locusts, and grasshoppers) and Holometabola, which diverged approximately 380 million years ago (Mya) [12], thus implying that its role in assembling germ plasm is a derived trait in higher insects (Figure 4). In support of this interpretation, we note that insect germ plasm itself is thought to be a derived trait within insects and unique to Holometabola [5], consistent with our observation that *Gryllus* possesses an *oskar* ortholog yet lacks germ plasm. Moreover, in *Drosophila* adults, *oskar* is expressed in the brain and is required for place learning, as are

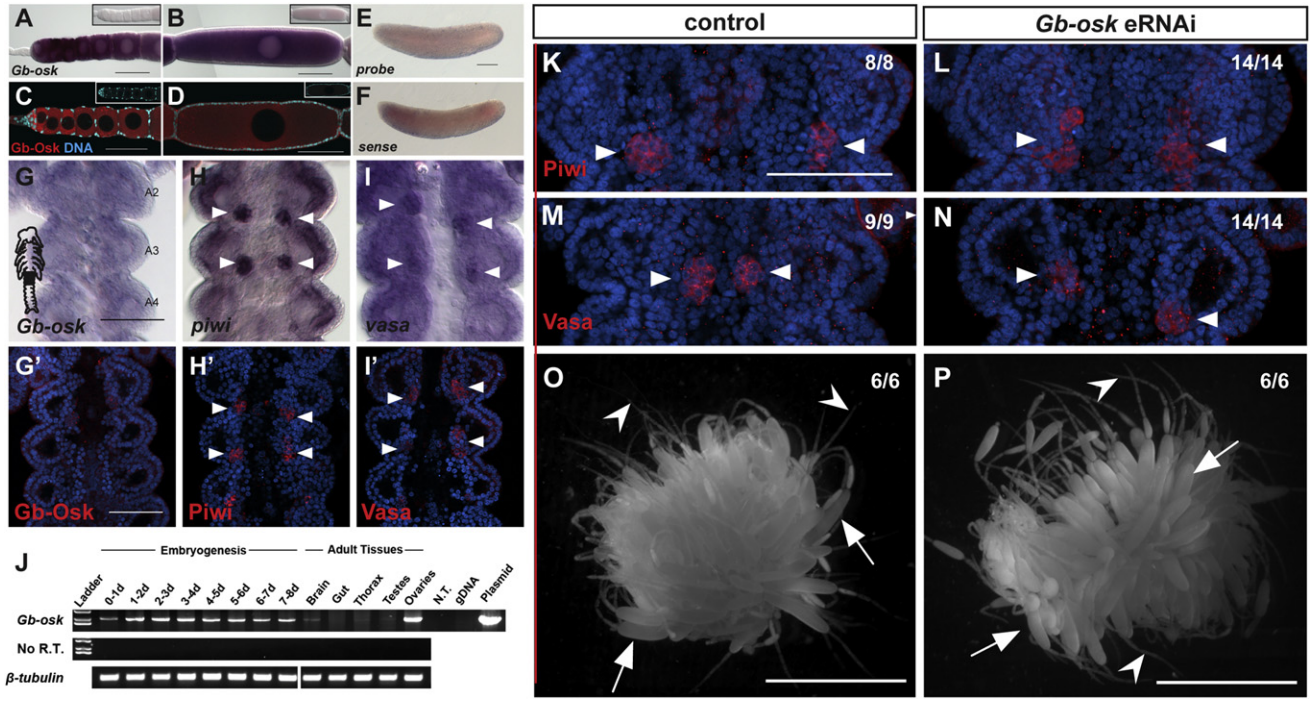

Figure 2. *Gb-oskar* mRNA and Protein Do Not Accumulate in Germ Plasm or Embryonic Germ Cells and Are Not Required for Germ Cell Formation or Development

(A–D) *Gb-oskar* mRNA (A and B) and protein (C and D) are expressed ubiquitously in oocytes and do not accumulate asymmetrically at the posterior. Insets show sense probe (A and B) and preimmune serum (C and D) controls. (E) *Gb-oskar* transcript levels are low and ubiquitous in blastoderm stage embryos. (F) Gb-oskar sense control. (G–I′) In fully segmented embryos, *Gb-oskar* mRNA (G) and protein (G′) are not enriched in embryonic germ cells, which express *piwi* and *vasa* mRNA (H and I) and protein (H′ and I′). Arrowheads in (H)–(I′) indicate germ cell clusters. A2, A3, and A4 indicate abdominal segments 2, 3, and 4. Black region of embryo schematic in (G) shows the region displayed in (G)–(I′). (J) RT-PCR analysis of *Gb-oskar* throughout embryogenesis and in different adult tissues. *β-tubulin* was used to ensure equal quantities of RNA template in the cDNA synthesis reaction and as a gel loading control. The amplified *Gb-oskar* band is 2,149 bp and was amplified with 35× PCR cycles. The highest levels of *Gb-oskar* are detected throughout embryogenesis and in adult ovaries. Lower levels are detected in the adult brain, and faint expression is detected in the adult thoracic muscles and testes. No expression is detected in the adult gut. N.T., no template control; gDNA, genomic DNA control; Plasmid, *Gb-oskar* amplified from the full-length plasmid clone; No R.T., no reverse transcriptase control. (K–N) Vasa- and Piwi-positive germ cells form in *Gb-oskar* eRNAi embryos (L and N) as in *DsRed* eRNAi controls (K and M). (P and O) *Gb-oskar* eRNAi embryos raised to adulthood form functional ovaries (P), which contain functional germaria (arrowheads) and late-stage oocytes (arrows) as in uninjected controls (O). Numbers indicate sample sizes. Left shows anterior in (A)–(E) and top shows anterior in (G)–(I′) and (K)–(N). Scale bar represents 100 μm in (A)–(M) and 5 mm in (N) and (O). Validation of all Gb-specific antibodies is shown in Figure S2; validation of *Gb-oskar* eRNAi is shown in Figure S3. Absence of a role for *Gb-oskar* in axial patterning is shown in Figure S3 and Table S1.

several other *Drosophila* genes with germline functions [4, 20], suggesting that these genes may have an ancient association with the nervous system.

Multiple *Drosophila* genes originally characterized for their role in germ cell development, including *nanos*, *pumilio*, and *Staufen*, have subsequently been shown to function in the nervous system, where they regulate translation in such processes as dendrite morphogenesis, synaptic growth, asymmetric neuroblast divisions, and neuronal specification [4, 21–23]. The co-occurrence of multiple germ plasm genes in the CNS of *D. melanogaster* raises the intriguing possibility that these genes may function within an evolutionarily conserved functional module [24], which could facilitate their co-option to a novel context such as holometabolous germ plasm. Consistent with this hypothesis, we find that *Gb-vasa* mRNA and protein are coexpressed with *Gb-oskar* in neuroblasts (Figures S2I–S2K), suggesting that a functional link between *oskar* and other germline genes predates the evolution of germ plasm. Moreover, expression of germline genes in the nervous system has also been observed in other insects belonging to both Hemimetabola (*piwi* in aphids [25]) and Holometabola (*vasa* in ants [26]).

If *oskar* were to acquire expression in germ cells due to its functional linkage with other germ plasm genes, an evolutionary change in its transcriptional, translational, or functional regulation might then have feasibly allowed its co-option to a critical function in the germline specification pathway. Consistent with this possibility, we note the presence of extremely low levels of *Gb-oskar* in *Gryllus* germ cells (Figures 2G and 2G′), although it appears to play no essential germ cell function (Figures 2K–2P). Co-option of *oskar* to assemble germ plasm probably involved molecular evolution of its regulation and function; accordingly, we find that *Gb-oskar* is not regulated by *Drosophila oskar* translational machinery in *Drosophila* oocytes or embryos (Figure S4, Table S2), suggesting that *oskar*'s translational regulation mechanisms have evolved extensively in the lineage leading to *Drosophila*. However, it is also possible that specific features of the *Gb-oskar* coding sequence, or its incompatibility with *Drosophila* UTRs, may have prevented the translation of Gb-Oskar in our transgenic experiments.

We have shown that *oskar* was present nearly 50 million years earlier in insect evolution than previously thought [3, 12] and must therefore have been lost several times in

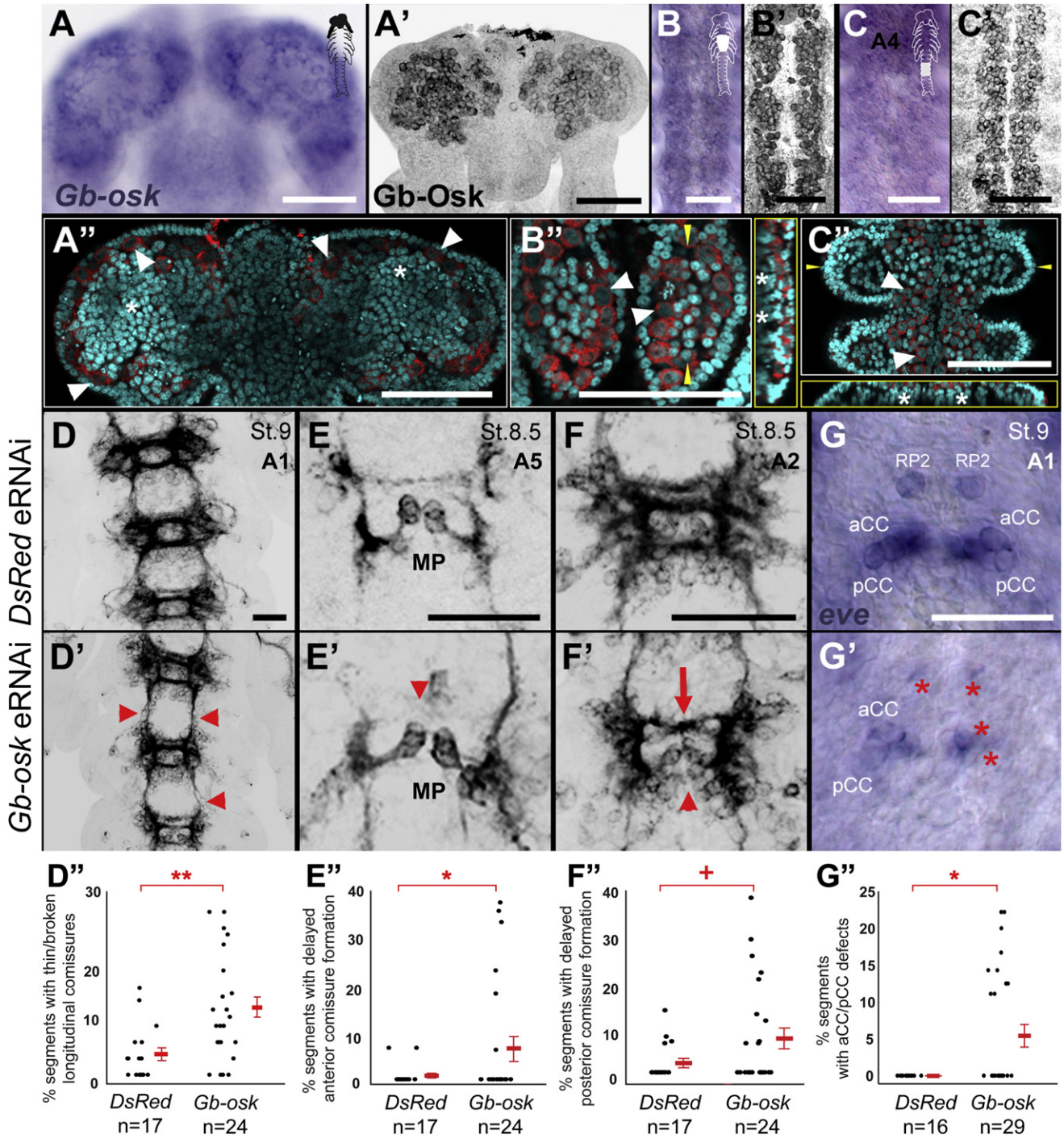

Figure 3. *Gb-oskar* Is Expressed in Neuroblasts and Is Required for Neural Development

(A– C″) *Gb-oskar* mRNA (A, B, and C) and protein (A′, B′, and C′) accumulate in neuroblasts of the brain (A and A′), thorax (T1–T3; B and B′), and abdomen (A4–A6; C and C′). (A″), (B″), and (C″) show single optical sections of Gb-Osk expression (red, Gb-Osk; cyan, nuclei), revealing the highest levels of Gb-Osk expression in neuroblasts (cells with large nuclei and diffuse chromatin; arrowheads) and absent or lower levels in neuroblast daughter cells (cells with smaller, denser nuclei; asterisks). Bright staining near midline of head in (A′) and (A″) is nonspecific staining of the extraembryonic membranes. Large panels of (B″) and (C″) show single optical sections through T3 and A5 neuromeres, respectively; anterior is on top in both central panels. Yellow framed boxes to the left and bottom of (B″) and (C″), respectively, show orthogonal sections at the plane indicated by yellow arrowheads in the large panels; in these orthogonal sections, ventral is on the right in (B″) and on top in (C″). White arrowheads indicate Gb-Osk-expressing neuroblasts immediately dorsal to the ectoderm and ventral to the underlying daughter neurons and neuronal precursors (asterisks), which show little to no expression of Gb-Osk. (D–F′) Ventral views of embryonic abdominal segments of *DsRed* eRNAi controls (D, E, and F) and *Gb-oskar* eRNAi in embryos of the same developmental stage (D′, E′, and F′) labeled with axonal marker anti-HRP. The percent of *Gb-oskar* eRNAi embryos that exhibit thin or broken longitudinal connectives (arrowheads) is 83.3% (D and D′). *Gb-oskar* eRNAi embryos show delayed formation of both anterior (E and E′) and posterior (F and F′) commissures (arrowheads) relative to the development of the midline precursors (MP). Abnormal or fused anterior commissures also appear in a greater proportion of *Gb-oskar* eRNAi embryos than in controls (arrow in F′). (G and G′) Formation of aCC and pCC neurons is impaired in *Gb-oskar* eRNAi embryos (asterisks) (G′) but never

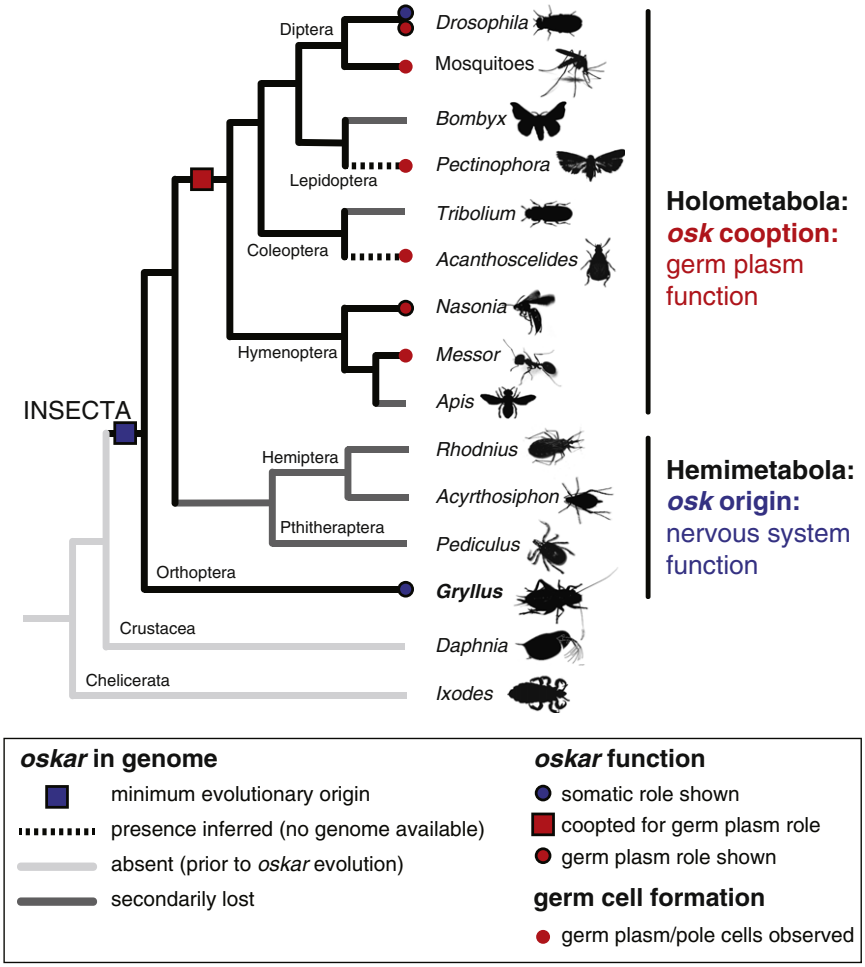

Figure 4. Phylogenetic Hypothesis of *oskar* Origin and Function across Arthropods

Species shown have sequenced genomes, allowing unambiguous determination of the presence or absence of an *oskar* ortholog; dotted lines indicate exceptions to this rule and show taxa in which pole cells and/or germ plasm have been observed but that lack available genome sequence. *oskar* is absent from the sequenced genomes of noninsect arthropods (light gray lines). Boxes indicate proposed origin of *oskar* in the last common ancestor of Holometabola and Hemimetabola (blue) and putative co-option of *oskar* to a germline role in the Holometabola (red). Circles indicate that *oskar* plays known roles in the nervous system (blue) or presumably in the germline (red); circles outlined in black indicate that there is functional evidence for the described role. Evidence for evolution of *oskar* translational regulation in the lineage leading to *D. melanogaster* is shown in Figure S4 and Table S2.

some insect lineages (Figure 4). Indeed, completely sequenced genomes of holometabolous insects lacking germ plasm or pole cells confirm that *oskar* has been lost in these lineages [3]. Germ cell specification via germ plasm is thought to have arisen independently in multiple bilaterian taxa [5], but how germ plasm evolved has remained unclear. Our results suggest a novel molecular mechanism for this process in insects: co-option of the *oskar* gene into the top of the germ plasm assembly hierarchy.

Experimental Procedures

Animal Husbandry, Gene Expression, and Functional Analysis

G. bimaculatus husbandry, gene expression analysis, RNAi experiments, egg-laying analysis, and axonal scaffold visualization were carried out as previously described [16].

Gene Cloning and Phylogenetic Analysis

Full-length *Gb-oskar* was recovered from a *G. bimaculatus* transcriptome and its identity confirmed by both Bayesian and Maximum Likelihood analysis. Details of sequence analysis are available in Supplemental Experimental Procedures.

Antibody Generation

Rabbit polyclonal antibodies were raised against an N-terminal and a C-terminal peptide from Gb-Oskar (Figures S1 and S2A) (Open Biosystems), recombinant proteins of full-length Gb-Vasa, and a 774 amino acid fragment of Gb-Piwi (McGill Biology CIAN facility). Details of antibody construction and validation are described in Supplemental Experimental Procedures.

Accession Numbers

The Genbank accession numbers for the *Gb-oskar*, *Gb-piwi-like*, and *Gb-tdrd7* sequences reported in this paper are JQ434102, JQ434103, and JQ434104, respectively.

Supplemental Information

Supplemental Information includes four figures, two tables, and Supplemental Experimental Procedures and can be found with this article online at http://dx.doi.org/10.1016/j.cub.2012.10.019.

Acknowledgments

NSF IOS-0817678 to C.G.E., DFG postdoctoral fellowship SCHW 1557/1-1 to E.E.S., and NSF predoctoral fellowships to B.E.-C. and J.R.S. supported

in controls (G). aCC/pCC are located in the corners where the longitudinal connectives meet the posterior commissure; these axonal scaffolds are visible in (G). The out-of-focus darkened spots adjacent to the in-focus aCC/pCC neurons are U/CQ neurons present ventral to the dorsally located aCC/pCC neurons. (D″, E″, F″, and G″) Quantification of neural defects illustrated in (D), (E), (F), and (G); thick red bars at the bottom of plots show mean values ± SE. Statistical significance of differences between treatments (red brackets) based on chi-square tests: $^{**}p < 0.001$, $^{*}p < 0.01$, $^{+}p < 0.025$. Anterior is shown on the top in all panels. Scale bar represents 100 μM in (A)–(C″) and 50 μM in (D)–(G″). Embryonic stage and/or the most anterior segment shown are indicated in top right corner in (C), (D), (E), (F), and (G); stages and segments shown in (D), (E), (F), and (G) apply to (D′), (E′), (F′), and (G′), respectively. Validation of *Gb-oskar* eRNAi is shown in Figures S2 and S3.

this work. We thank Elke Küster-Schöck of the McGill Biology Cell Imaging and Analysis Network (Canada) for assistance with antibody creation, Andrés Leschziner for western blot assistance, Anne Ephrussi, Satoru Kobayashi, Sam Kunes, and Akira Nakamura for reagents, and members of the Extavour laboratory for discussion.

Received: August 22, 2012
Revised: September 16, 2012
Accepted: October 9, 2012
Published online: November 1, 2012

References

1. Ephrussi, A., and Lehmann, R. (1992). Induction of germ cell formation by *oskar*. Nature *358*, 387–392.
2. Smith, J.L., Wilson, J.E., and Macdonald, P.M. (1992). Overexpression of *oskar* directs ectopic activation of *nanos* and presumptive pole cell formation in *Drosophila* embryos. Cell *70*, 849–859.
3. Lynch, J.A., Ozüak, O., Khila, A., Abouheif, E., Desplan, C., and Roth, S. (2011). The phylogenetic origin of *oskar* coincided with the origin of maternally provisioned germ plasm and pole cells at the base of the Holometabola. PLoS Genet. *7*, e1002029.
4. Dubnau, J., Chiang, A.-S., Grady, L., Barditch, J., Gossweiler, S., McNeil, J., Smith, P., Buldoc, F., Scott, R., Certa, U., et al. (2003). The *staufen/pumilio* pathway is involved in *Drosophila* long-term memory. Curr. Biol. *13*, 286–296.
5. Extavour, C.G., and Akam, M.E. (2003). Mechanisms of germ cell specification across the metazoans: epigenesis and preformation. Development *130*, 5869–5884.
6. Lehmann, R., and Nüsslein-Volhard, C. (1986). Abdominal segmentation, pole cell formation, and embryonic polarity require the localized activity of *oskar*, a maternal gene in *Drosophila*. Cell *47*, 141–152.
7. Mahowald, A.P. (2001). Assembly of the *Drosophila* germ plasm. Int. Rev. Cytol. *203*, 187–213.
8. Ephrussi, A., Dickinson, L.K., and Lehmann, R. (1991). Oskar organizes the germ plasm and directs localization of the posterior determinant *nanos*. Cell *66*, 37–50.
9. Anantharaman, V., Zhang, D., and Aravind, L. (2010). OST-HTH: a novel predicted RNA-binding domain. Biol. Direct *5*, 13.
10. Callebaut, I., and Mornon, J.-P. (2010). LOTUS, a new domain associated with small RNA pathways in the germline. Bioinformatics *26*, 1140–1144.
11. Webster, P.J., Suen, J., and Macdonald, P.M. (1994). *Drosophila virilis oskar* transgenes direct body patterning but not pole cell formation or maintenance of mRNA localization in *D. melanogaster*. Development *120*, 2027–2037.
12. Gaunt, M.W., and Miles, M.A. (2002). An insect molecular clock dates the origin of the insects and accords with palaeontological and biogeographic landmarks. Mol. Biol. Evol. *19*, 748–761.
13. Wheeler, W.M. (1893). A contribution to insect morphology. J. Morphol. *8*, 1–160.
14. Johannsen, O.A., and Butt, F.H. (1941). Embryology of Insects and Myriapods (New York: McGraw-Hill).
15. Kim-Ha, J., Smith, J.L., and Macdonald, P.M. (1991). *oskar* mRNA is localized to the posterior pole of the *Drosophila* oocyte. Cell *66*, 23–35.
16. Kainz, F., Ewen-Campen, B., Akam, M., and Extavour, C.G. (2011). Notch/Delta signalling is not required for segment generation in the basally branching insect *Gryllus bimaculatus*. Development *138*, 5015–5026.
17. Stollewerk, A., and Simpson, P. (2005). Evolution of early development of the nervous system: a comparison between arthropods. Bioessays *27*, 874–883.
18. Ikeshima-Kataoka, H., Skeath, J.B., Nabeshima, Y., Doe, C.Q., and Matsuzaki, F. (1997). Miranda directs Prospero to a daughter cell during *Drosophila* asymmetric divisions. Nature *390*, 625–629.
19. Thomas, J.B., Bastiani, M.J., Bate, M., and Goodman, C.S. (1984). From grasshopper to *Drosophila*: a common plan for neuronal development. Nature *310*, 203–207.
20. Chintapalli, V.R., Wang, J., and Dow, J.A. (2007). Using FlyAtlas to identify better *Drosophila melanogaster* models of human disease. Nat. Genet. *39*, 715–720.
21. Li, P., Yang, X., Wasser, M., Cai, Y., and Chia, W. (1997). Inscuteable and Staufen mediate asymmetric localization and segregation of *prospero* RNA during *Drosophila* neuroblast cell divisions. Cell *90*, 437–447.
22. Menon, K.P., Sanyal, S., Habara, Y., Sanchez, R., Wharton, R.P., Ramaswami, M., and Zinn, K. (2004). The translational repressor Pumilio regulates presynaptic morphology and controls postsynaptic accumulation of translation factor eIF-4E. Neuron *44*, 663–676.
23. Ye, B., Petritsch, C., Clark, I.E., Gavis, E.R., Jan, L.Y., and Jan, Y.N. (2004). *nanos* and *pumilio* are essential for dendrite morphogenesis in *Drosophila* peripheral neurons. Curr. Biol. *14*, 314–321.
24. Wagner, G.P., Pavlicev, M., and Cheverud, J.M. (2007). The road to modularity. Nat. Rev. Genet. *8*, 921–931.
25. Lu, H.L., Tanguy, S., Rispe, C., Gauthier, J.P., Walsh, T., Gordon, K., Edwards, O., Tagu, D., Chang, C.C., and Jaubert-Possamai, S. (2011). Expansion of genes encoding piRNA-associated Argonaute proteins in the pea aphid: diversification of expression profiles in different plastic morphs. PLoS ONE *6*, e28051.
26. Khila, A., and Abouheif, E. (2010). Evaluating the role of reproductive constraints in ant social evolution. Philos. Trans. R. Soc. Lond. B Biol. Sci. *365*, 617–630.

Current Biology, Volume *22*

Supplemental Information

oskar Predates the Evolution of Germ Plasm in Insects

Ben Ewen-Campen, John R. Srouji, Evelyn E. Schwager, and Cassandra G. Extavour

Supplemental Inventory

- *Supplemental Data*
    - Figures S1-S4
    - Tables S1 and S2
- *Supplemental Experimental Procedures*
- *Supplemental References*

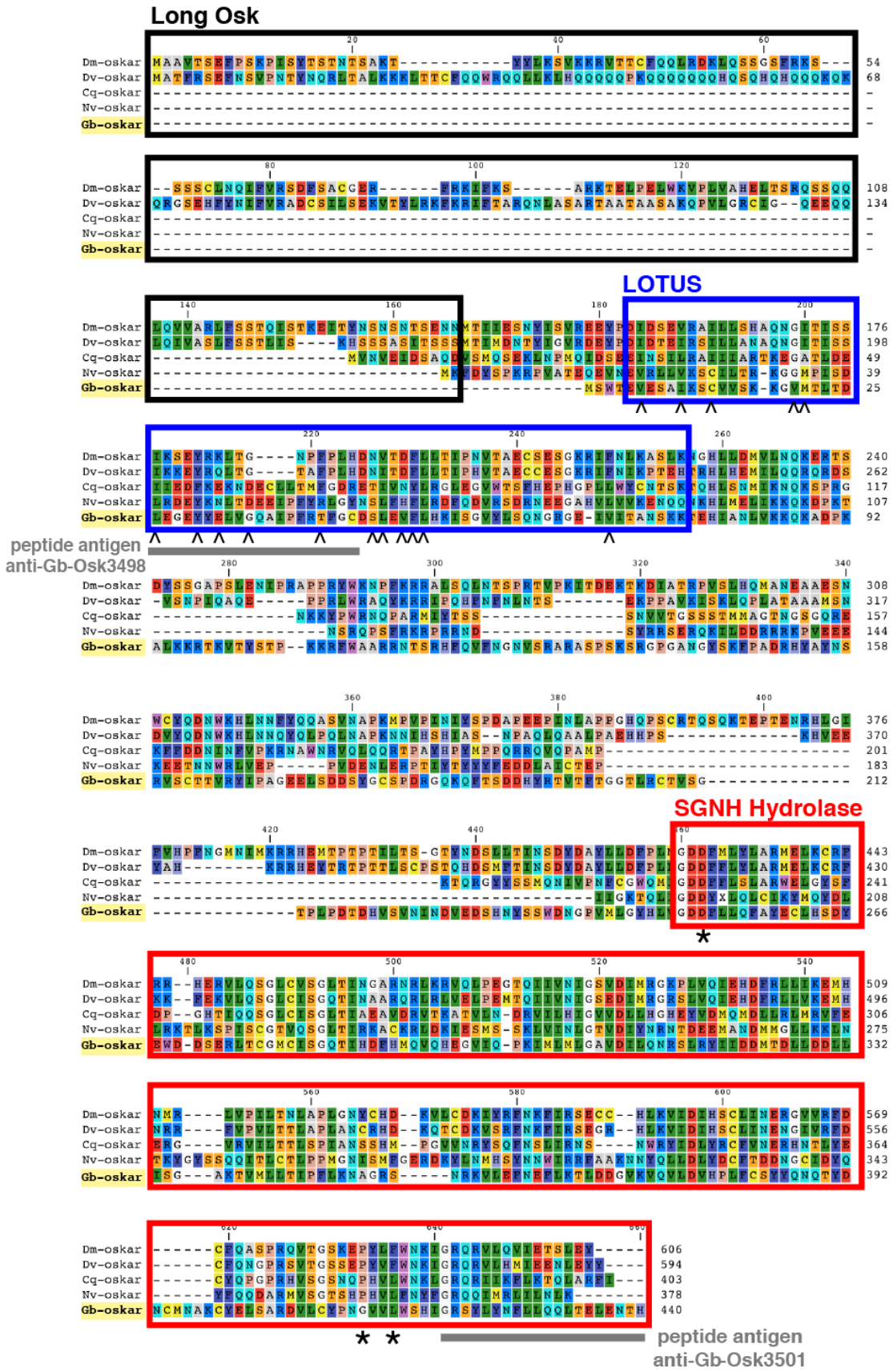
Long Osk
LOTUS
peptide antigen
anti-Gb-Osk3498
SGNH Hydrolase
peptide antigen
anti-Gb-Osk3501

Figure S1, related to Figure 1. ClustalW alignment of Gb-Oskar with known *oskar* orthologs. Gb-Oskar contains the LOTUS (*aka* OST-HTH) domain (blue box) and the SGNH hydrolase domain (red box) that are characteristic of Oskar orthologs. The Long Osk domain (black box) is only present in Oskar orthologs from Drosophilid species. Residues are colored using the RasMol color scheme to indicate physicochemical properties. Structurally conserved residues within the LOTUS domain are indicated with carets [1, 2]. Indicated with astrices are the positions of the serine, aspartate, and histidine residues (notably absent in Oskar) that constitute the catalytic triad in functional hydrolases [1]. The two peptide antigens used to generate Gb-Oskar antibodies are indicated in grey. Species (accession IDs): *Dm = Drosophila melanogaster* (AAF54306.1), *Dv = Drosophila virilis* (AAA28426.1), *Cq = Culex quinquefasciatus* (ACB20969.1)*; Nv = Nasonia vitripennis* (ADK94458.1), *Gb = Gryllus bimaculatus* (JQ434102).

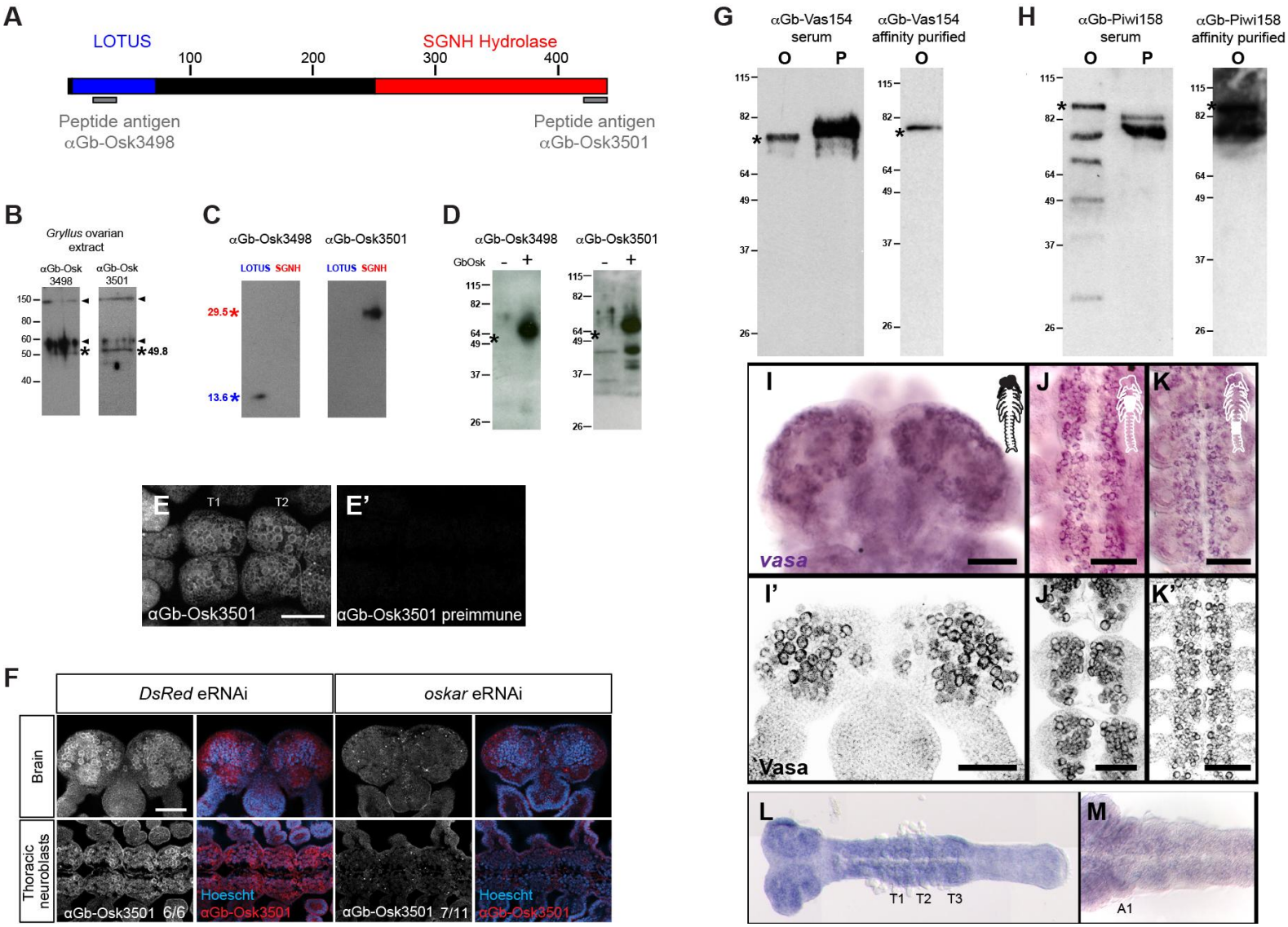
A
LOTUS
SGNH Hydrolase
100
200
300
400
Peptide antigen
αGb-Osk3498
Peptide antigen
αGb-Osk3501
B
Gryllus ovarian extract
αGb-Osk 3498
αGb-Osk 3501
150
80
60
50
40
49.8
C
αGb-Osk3498
αGb-Osk3501
LOTUS SGNH
LOTUS SGNH
29.5
13.6
D
αGb-Osk3498
αGb-Osk3501
GbOsk - +
- +
115
82
64
49
37
26
E
T1
T2
αGb-Osk3501
E'
αGb-Osk3501 preimmune
F
DsRed eRNAi
oskar eRNAi
Brain
Thoracic neuroblasts
αGb-Osk3501 6/6
Hoescht
αGb-Osk3501
αGb-Osk3501 7/11
Hoescht
αGb-Osk3501
G
αGb-Vas154 serum
αGb-Vas154 affinity purified
O
P
O
115
82
64
49
37
26
H
αGb-Piwi158 serum
αGb-Piwi158 affinity purified
O
P
O
115
82
64
49
37
26
I
vasa
J
K
I'
Vasa
J'
K'
L
T1 T2 T3
M
A1

Figure S2, related to Figures 2, 3. Validation of rabbit αGb-Oskar, αGb-Vasa and αGb-Piwi antibodies. (A) Schematic of Gb-Oskar, showing the location of the LOTUS (blue) and SGNH hydrolase (red) domains, and the N- and C-terminal peptides used to generate αGb-Osk3498 and αGb-Osk3501 respectively (grey). **(B)**Western blot of *Gryllus* ovarian extract probed with αGb-Oskar antibodies. Bands are detected at the predicted weight of Gb-Oskar (black asterisk: 49.8 kDa). **(C)** Western blot of purified recombinant LOTUS and SGNH domains from Gb-Oskar probed with αGb-Oskar antibodies. αGb-Osk3498 specifically recognized the LOTUS domain (blue askterisk indicates expected size of 13.6 kDa) but not the SGNH hydrolase domain (red asterisk indicates expected size of 29.6 kDa). Conversely, αGb-Osk3501 specifically recognized the SGNH hydrolase domain but not the LOTUS domain. **(D)** Western blot of whole cell lysate of *E. coli* expressing full length Gb-Oskar. The predominant band is slightly larger than expected (black asterisk 49.8 Kda), as in (**A**). (-) uninduced *E. coli*, (+) induced *E. coli*.**(E-E")** The expression of Gb-Oskar in neuroblasts (here shown in thoracic segments T1 and T2) is only seen using the final bleed serum (**E**), and is not present using the preimmune serum (**E'**). (**F**) Gb-Oskar immunostaining in brain (top row) and thoracic neuroblasts (bottom row) is greatly reduced following *Gb-oskar* eRNAi, validating the specificity of the antiserum and the efficacy of the RNAi knockdown. Sample sizes are given at the bottom of each panel. Anterior is to the left in (**E-E"**) and in (**F**) bottom row; anterior is up in (**F**) top row. Scale bars = 100 μM. (**G**) Western blots of unpurified αGbVas154 serum on *Gryllus* ovarian extracts (O) and purified protein (P). Serum used at 1:5,000 recognizes a band of the expected size (asterisk: 75kDa) and a smaller secondary band from ovarian extracts. Following affinity purification against recombinant Gb-Vasa protein used at 1:500, the antibody recognizes a single band of the expected size from ovarian extracts (O). (**H**) Western blots of unpurified αGbPiwi158 serum on *Gryllus* ovarian extracts (O) and purified protein (P). Serum used at 1:2,000 recognizes a band of the expected size (asterisk: 92kDa) and several smaller secondary bands from ovarian extracts. Following affinity purification agasint Protein-A, serum used at 1:500 shows reocgnition of most smaller secondary bands is abolished and the antibody strongly recognizes a band of the expected size as well as a slightly smaller secondary band from ovarian extracts (O). In situ hybridization for *Gb-vasa* (**I-K**) and antibody staining with αGbVas154 (**I'-K'**) shows expression of *Gb-vasa* transcript and protein in neuroblasts of the embryonic brain (**I, I'**), thorax (**J, J'**) and abdomen (**K, K'**) in Stage 9 embryos. *Gb-oskar* expression increases in the ectodermal neuroblast precursor territory just prior to neuroblast formation at Stage 5 (**L**) and in newly forming neuroblasts at Stage 6 (**M**). Scale bar = 100 μM.

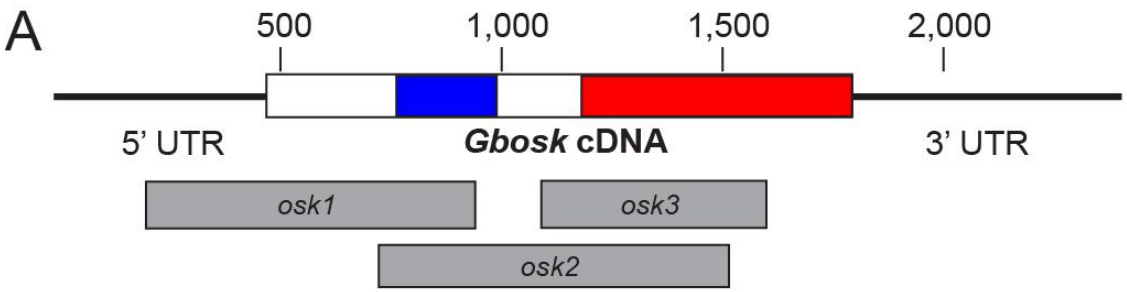

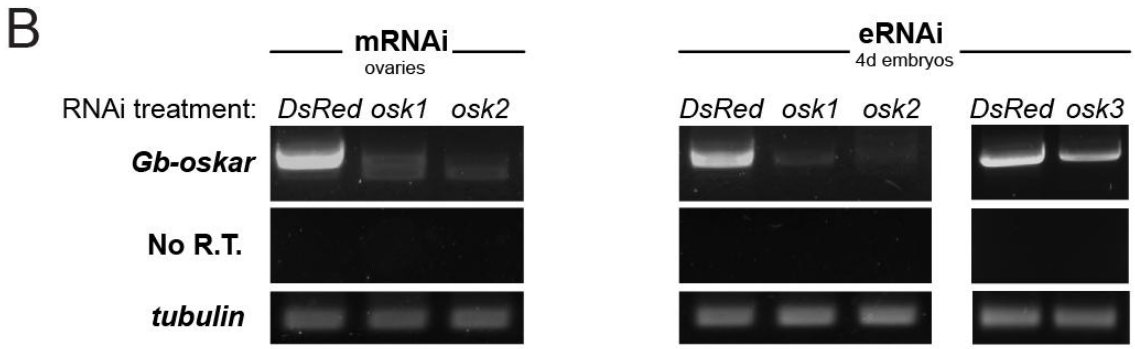

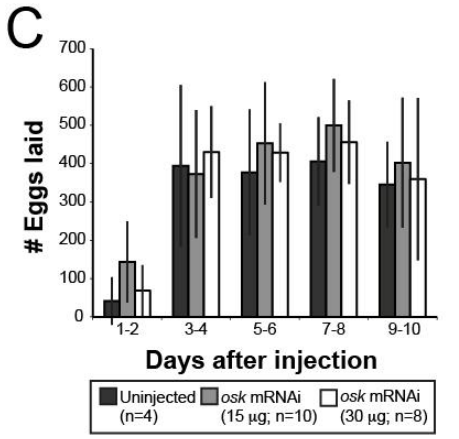

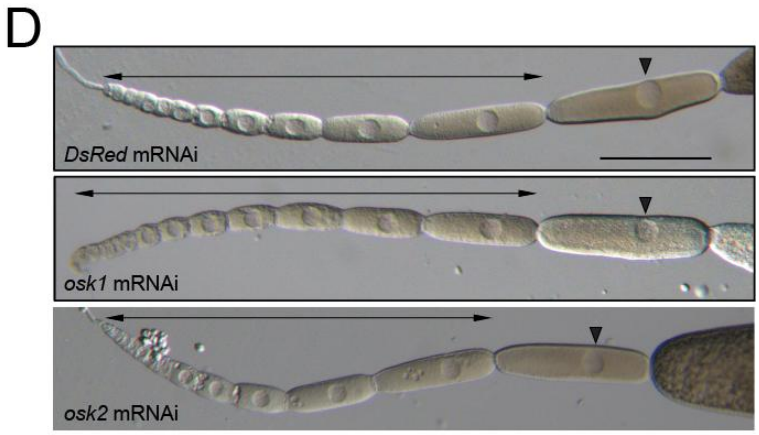

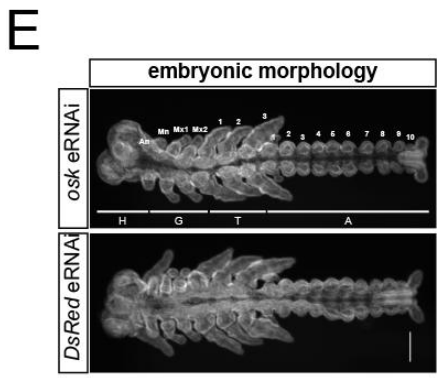

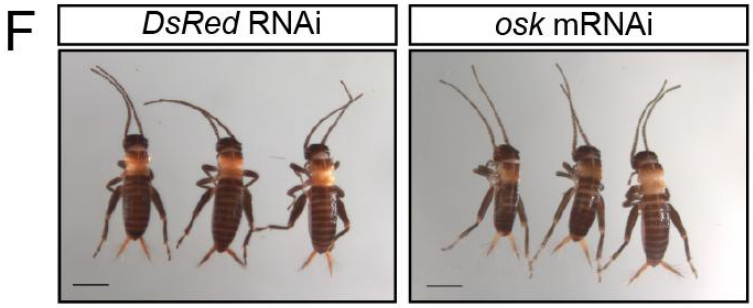

dsRNA	Hatching rate (%)	Wild type morphology (%)
osk1	435 / 565 (77%)	435 / 435 (100%)
osk2	136 / 216 (63%)	136 / 136 (100%)
DsRed	64 / 78 (82%)	64 / 64 (100%)

Figure S3, related to Figures 2, 3. Validation and phenotypes of *Gb-oskar* RNAi. (**A**) Schematic of the three dsRNA fragments used for *Gb-oskar* RNAi experiments. Blue and red regions indicate locations of the LOTUS and SGNH hydrolase domains respectively. Grey boxes indicate fragments used for RNAi treatments. (**B**) Semi-quantitative PCR analysis of *Gb-oskar* levels in negative control (*DsRed*), *osk1* and *osk2* RNAi treatments. Maternal RNAi (mRNAi) greatly reduces *Gb-oskar* transcript levels in ovaries of injected females even 10 days after injection (left panel). Near-complete reduction of *Gb-oskar* transcript in embryos via embryonic RNAi (eRNAi) with fragments *osk1* and *osk2*, and a lesser reduction with fragment *osk3*, persists through until at least 4 days after egg laying (right panel). No R.T. = No reverse transcriptase control to ensure the absense of genomic DNA. *β-tubulin* serves as a loading and RNAi specificity control**. (C)** Average daily egg-laying rate is not significantly different between *Gb-oskar* mRNAi-injected females and controls, at two different concentrations of *Gb-oskar* dsRNA. Error bars indicate 95% confidence interval. *osk1* and *osk2* results are pooled for each concentration, as no significant differences were seen between these treatments. (**D**) *Gb-oskar* mRNAi does not disrupt oogenesis or ovarian morphology. Double-headed arrows indicate that oocytes at stages of oogenesis are present in RNAi treated ovaries as well as controls. Arrowhead indicates the posterior localization of the oocyte nucleus, which indicates normal oocyte patterning [3]. **(E)** Nuclear stain of *Gb-oskar* eRNAi embryos reveals wild type anterior-posterior patterning compared to controls. **(F)** *Gb-oskar* mRNAi hatchlings (right panel) do not display obvious morphological defects compared to controls (left panel). Hatching rate is not significantly different between *Gb-oskar* mRNAi embryos (right panel) and controls (left panel). Scale bars = 100 μM in D-E, 1 mm in F.

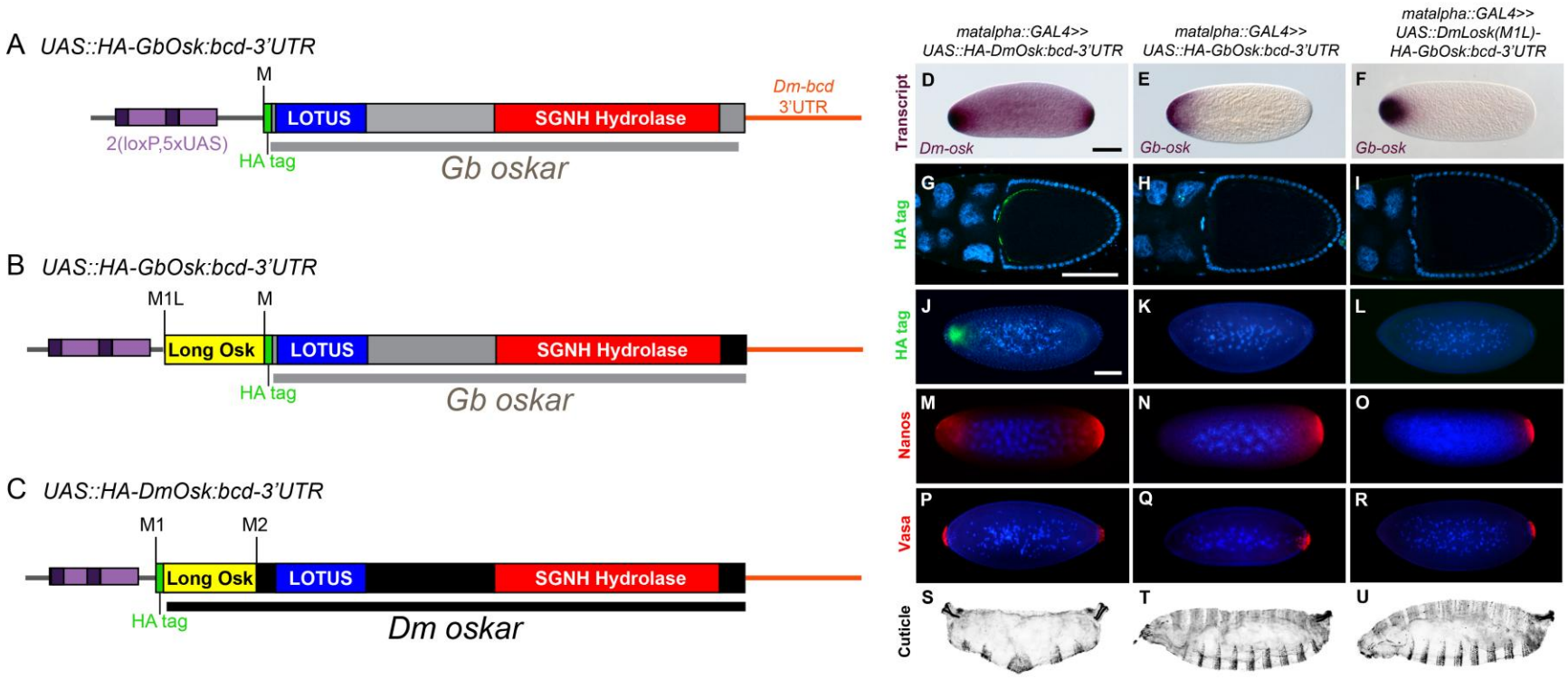
A UAS::HA-GbOsk:bcd-3'UTR
M
LOTUS
SGNH Hydrolase
Dm-bcd 3'UTR
2(loxP,5xUAS)
HA tag
Gb oskar
B UAS::HA-GbOsk:bcd-3'UTR
M1L
M
Long Osk
LOTUS
SGNH Hydrolase
HA tag
Gb oskar
C UAS::HA-DmOsk:bcd-3'UTR
M1
M2
Long Osk
LOTUS
SGNH Hydrolase
HA tag
Dm oskar
matalpha::GAL4>> UAS::HA-DmOsk:bcd-3'UTR
matalpha::GAL4>> UAS::HA-GbOsk:bcd-3'UTR
matalpha::GAL4>> UAS::DmLosk(M1L)-HA-GbOsk:bcd-3'UTR
Transcript
HA tag
HA tag
Nanos
Vasa
Cuticle
D
E
F
G
H
I
J
K
L
M
N
O
P
Q
R
S
T
U
Dm-osk
Gb-osk
Gb-osk

Figure S4, related to Figure 4. Schematic of constructs used for transgenic *D. melanogaster*, which show that *Gb-oskar* and *DmLosk(M1L)*:*GbOskar* transgenes are transcribed and localized but not translated in *Drosophila* ovaries or embryos. Full length cDNAs of *Gb-oskar* (**A**), *Gb-oskar* downstream of *Dm-Losk*(M1L) (**B**) or full length *Dm-osk* (**C**) were fused to an N-terminal HA tag fused to the *Dm-bicoid* 3'UTR sequence. Constructs were cloned into the pValium22 vector for site-directed insertion via the ΦC31 targeted transgenesis system . HA-tagged *Dm-osk* (D, G, J, M, P, S), *Gb-oskar* (E, H, K, N, Q, T), or DmLosk(M1L)-*Gb-osk* (F, I, L, O, R, U) fused to the *bicoid* 3'UTR were expressed in transgenic *D. melanogaster* with a maternal GAL4 driver (matalpha). In situ hybridization for *Dm-osk* (D) or *Gb-oskar* (E, F) shows that all transcripts are localized to the anterior of early embryos. Dm-Oskar but not Gb-Oskar protein is translated in oocytes (G, H, I) and early embryos (J, K, L). Ectopic Dm-Osk causes anterior localization of Nanos (M) and ectopic Vasa-positive pole cells (P) and a bicaudal phenotype revealed in larval cuticle preparations (S). Absence of detectable ectopic Gb-Oskar (H, I, K, L) is correlated with absence of ectopic Nanos (N, O), Vasa or pole cells (Q, R) and larval morphology is wild type (T, U). In all panels anterior is to the left, scale bar = 100 μm.

Table S1, related to Figure 2. Anterior-posterior axis phenotypes in *Gb-oskar* RNAi embryos.

RNAi method	dsRNA injected	# embryos injected[1]	# developed (%)	# surviving embryos with morphological abnormalities (%)
Maternal (mRNAi)	*osk1*	123	75 (61.0%)	0
	osk2	52	23 (44.2%)	0
	caudal	589	486 (82.5%)	321 (66.0%)
	DsRed	135	81 (60%)	0
Embryonic (eRNAi)	*osk1*	125	101 (80.8%)	0
	osk2	67	41 (61.2%)	0
	osk3	150	53 (35.3%)	0
	caudal	168	131 (78.0%)	110 (84.0%)
	DsRed	74	65 (87.8%)	0
	DsRed[2]	85	65 (76.5%)	0
	uninjected	90	64 (71.1%)	0

1. For maternal RNAi, this number refers to number of eggs dissected.

Table S2, related to Figure 4. Effect of the *Gb-oskar* transgenes in *D. melanogaster* using the bicoid 3' UTR.

Maternal genotype	bicaudal phenotype / total (%)	anterior Vasa-positive cells / total (%)
matalpha >> HA-Dm-osk:bcd3'UTR	63 / 76 (82.9%)	42 / 60 (70%)
matalpha >> HA-Gb-osk:bcd3'UTR	0 / 73 (0%)	0 / 54 (0%)
matalpha >> DmLosk(M1L):HA-Gb-osk:bcd3'UTR	0 / 91 (0%)	0 / 61 (0%)
matalpha >> DmOsk(M1L):bcd3'UTR	20 / 26 (76.9%)	14 / 28 (50%)[1]

1. Of the 14 embryos with ectopic germ cells, six (42.8%) did not form at the anterior pole, but instead formed slightly more posteriorly.

Supplemental Experimental Procedures

Gb-Oskar Identification and Phylogenetic Analysis

Gb-oskar was recovered from a de novo transcriptome generated using 454 Titanium sequencing. A 1,323 bp predicted full length *Gb-oskar* sequence was assembled from 695 raw reads (from a total of 4.2 million reads in the transcriptome), including additional 5' and 3' UTR sequence (462 bp and 607 bp, respectively). Our transcriptome assembly also contained a predicted alternate isoform of *Gb-oskar* that includes an additional 162 bp of sequence between the LOTUS and SGNH hydrolase domains. However, RT-PCR failed to amplify this larger product, and the additional sequence was not conserved in any other *oskar* orthologue. We therefore focused on the smaller of these two predicted isoforms, which we have confirmed is transcribed during *Gryllus* development by RT-PCR (Fig. 2J). Portions of *Gryllus piwi* and *tdrd7* orthologues were also found in our *Gryllus* transcriptome, and *Gryllus vasa* and *even-skipped* were cloned based on published sequence (AB378065, AB120736). All new sequence data have been submitted to NCBI (GenBank Accessions JQ434102-4).

In the course of performing reciprocal best BLAST hit analysis, we found that *Nasonia vitripennis oskar* (Nv-Osk, ADK94458.1), unlike *oskar* orthologues from *D. melanogaster* (AAF54306.1)*, Culex quinquefasciatus* (ACB20969.1)*, Aedes aegypti* (ABC41128.1)*, Anopheles gambiae* (ABC54566.1)*, and Messor pergandei* (ADM07366.1), retrieved a best hit against the *Gryllus* transcriptome sequence for *Gb-tdrd7* (e-value = 5e-11). However, this BLAST hit only extended over the LOTUS domain (amino acids 14-120), which is conserved in both *oskar* and *tdrd7* genes, while the second best hit, *Gb-oskar* (e-value = 2e-10), extended over both the LOTUS and SGNH hydrolase domain (amino acids 19-106 and 183-375 of the query). Further, *Gb-oskar* retrieves Nv-Osk as its top hit against the *N. vitripennis* proteome. We therefore concluded that across the length of the gene *Nv-oskar* is more similar to *Gb-oskar* than to *Gb-tdrd7*, a result that agrees with all other known *oskar* orthologues as well as our phylogenetic analysis (Fig. 1B).

Amino acid identity conservation (i.e. percentage of sequences containing an identical amino acid at a given alignment position) and physicochemical conservation were calculated using JalView [25].

To estimate a gene tree of *oskar* and *tdrd7* genes, *Gb-oskar* and *tdrd7* were aligned to their publically available orthologues using MUSCLE [26] (Fig. S1). Although *oskar* orthologues have been bioinformatically predicted in several recently sequenced Hymenopterans (retrievable at http://hymenopteragenome.org/ant_genomes/?q=blast), we only included those from *N. vitripennis* [NP_001234884.1] and *M. pergandei* [ADM07366.1] in our phylogenetic analysis, as these have been experimentally validated as true *oskar* orthologues [3]. Regions of uncertain alignment were removed using GBlocks [27] with the least stringent settings, which produced an alignment containing 294 amino acids. A gene tree for *oskar* and *tdrd7* was estimated under both Bayesian and maximum likelihood criteria. The "mixed" model of amino acid evolution was used in MrBayes v3.1.2 [28] to choose the optimal model for amino acid evolution for both this and the maximum likelihood tree. MrBayes selected the WAG model [29] with a probability of 1.0. Two runs of four independent MCMC chains each were executed for 2 million generations, sampling trees every 1,000 generations and the first 250,000 generations discarded as burn-in. The average standard deviation of split frequencies between the two runs fell below 0.01 after 154,000 generations, indicating that the two chains had converged. Maximum likelihood analysis

was estimated using RAxML-MPI v7.2.8. 2000 runs from independent starting trees were executed under the WAG model of protein evolution with gamma distribution of rate heterogeneity to simultaneously estimate the best scoring tree and perform rapid bootstrap analysis. All tree estimations were conducted on the Odyssey Cluster (Harvard University), supported by the FAS Sciences Division Research Computing group.

Gb-Oskar Antibody Generation

Two rabbit polyclonal antibodies were raised against an N-terminal peptide DLEGEYYELVGQAIPFRTFGC (αGb-Osk3498) and a C-terminal peptide GRSYLYNFLLQQLTELENTH (αGb-Osk3501) from Gb-Oskar (Figs. S1, S2A) (Open Biosystems, Inc., Alabama). Rabbits were boosted on days 14, 28, 42 and 82 after initial injection, and the final bleed was performed on day 138. Specificity was tested using Western blot analysis and immunostaining (Fig. S2B-F).

To prepare *Gryllus* ovaries for Western blotting, ~30-50 ovarioles were homogenized in 300 µL of 5X SDS loading buffer, boiled for 5 minutes at 95-100ºC, and stored at -20ºC until use. 1:10 and 1:100 dilutions of this homogenate, run in adjacent wells, were used in Western blots. For purified Gb-Oskar domains, 10 µg of purified protein were run. For whole-cell lysates containing full-length bacterially expressed Gb-Oskar, cells were grown (either with or without induction) overnight at 20ºC, and OD600 readings were used to calculate equal volumes of induced versus uninduced cells.

For Western blotting, samples were separated on a 12% acrylamide SDS-PAGE gel in running buffer (25 mM Tris base, 192 mM glycine, 0.1% w/v SDS) at ~180V for approximately one hour and then transferred to a nitrocellulose membrane (0.2 µm pore size, BIO-RAD cat. # 162-0112) at ~300V for 90-120 minutes at 4º C in transfer buffer (25 mM Tris base, 192 mM glycine, 0.1% w/v SDS, 20% v/v methanol). Ponceau S staining was used to verify that equal volumes were loaded in each lane and had transferred properly. Blots were blocked in 5% BSA + 5% milk powder for at least 30 minutes, and then incubated overnight with primary antibodies (1:500 dilution). Blots were washed at least 5 x 5 minutes in TBST (20 mM Tris pH 7.5, 500 mM NaCl, 0.05% (v/v) Tween-20) and then incubated with donkey anti-rabbit HRP-coupled secondary antibody (Jackson Laboratories, 1:5,000 dilution) in block for two hours. After 5 x 5 minute washes in TBST, the secondary antibody was detected with SuperSignal West Pico Chemiluminescent substrate (ThermoScientific) following manufacturer's protocols. Signal was visualized using Kodak BioMax film, and exposures were tested at 10 seconds, 1 minutes, 5 minutes, and 10 minutes to optimize exposure.

Both antibodies recognized proteins of the predicted size (asterisk in Fig. S2B) from *Gryllus* ovary extracts, as well as additional species of larger molecular weights (arrowheads in Fig. S2B), suggesting possible post-translational modification as has been reported for *Drosophila* Oskar [30]. Western blot analysis showed that as predicted, the αGb-Osk3501 serum recognized the C-terminal SGNH hydrolase domain and not the N-terminal LOTUS domain; conversely, the αGb-Osk3498 serum recognized the LOTUS domain and not the SGNH hydrolase domain (Fig. S2C). Both antibodies also recognized bacterially expressed full length Gb-Oskar at a slightly higher MW than predicted (Fig. S2D). The staining pattern seen in whole mount immunostained *Gryllus* embryos was not detected in pre-immune serum (Fig. S2E', E"), and was abolished by *oskar* RNAi (Fig. S2F).

Gb-Vasa and Gb-Piwi Antibody Generation

Rabbit polyclonal antibodies were raised against recombinant *Gryllus* Vasa and Piwi protein fragments (McGill Biology CIAN facility, Canada). Full-length *Gryllus vasa* (amino acids 2-649) and a fragment of *Gryllus piwi* (774 C-terminal amino acids ending at the stop codon) were each cloned into the pET151/dTOPO expression vector (Invitrogen Cat No. K151-01), thus introducing an N-terminal 6X-polyhistidine tag. Protein expression was induced in *E. coli* BL21 (DE3) by addition of IPTG to a final concentration of 0.25 mM and incubated at 30°C for 4 hrs. The overexpressed proteins were highly insoluble, so the cell pellets were disrupted by sonication in non-denaturing buffer, and soluble fraction were separated by centrifugation and discarded. The pellet was dissolved in 8 M urea (crude prep). Crude preps were further purified by SDS gel-purification. Protein bands were excised from the gel after reverse staining with zinc chloride and the proteins were collected by electroelution. Acetone precipitation was performed and the precipitated protein was washed and redissolved in 8M urea. Protein concentration was adjusted to 1-2 mg/ml for injection. Rabbits were injected using a standard 80-day protocol with three boosts after the initial injection; final bleed was performed after 87 days. The serum was processed by addition of NaN3 to 0.02% (w/v). Both antibodies were then affinity purified: αGb-Vasa was purified against bacterially expressed Gb-Vasa protein, and αGb-Piwi was purified with Protein A (Primm Biotech, Cambridge MA).

The CIAN facility determined specificity prior to purification using Western blot analysis (A-B, left blots), and we repeated this analysis following affinity purification using the above protocol (Fig. S2G-H, right blots).

In situ Hybridization and Antibody Staining

In situ hybridizations and antibody stainings were performed as described in [4]. Four different DIG-labeled fragments of *Gb-oskar* were used as in situ probes (ranging from 742 to 2,103 bp in size), all of which gave consistent staining results. *Gb-piwi* and *Gb-vasa* in situ probes were 781 bp and 1,953 bp, respectively. Probes were used at between 0.5-2 μg/μl during hybridization. For immunostainings, all species-specific primary antibodies used were used at a final dilution of 1:300. αGb-Oskar was preabsorbed against Oregon R *Drosophila* mixed stage embryos for 90 minutes at room temperature prior to staining to reduce background. Secondary antibodies used were goat anti-rabbit or goat anti-mouse coupled to Alexa 555, Alexa 488 or Alexa 647 (Invitrogen) at 1:1,000. Nuclei were counterstained with Hoechst 33342 at 1:5000 of a 10mg/ml stock solution. Cy3 conjugated anti-HRP (gift of Sam Kunes, Harvard University, MA, USA) was used at 1:50.

Injections for RNA Interference (RNAi)

Maternal and embryonic injections of dsRNA were carried out as described in [4]. To synchronize adult female age for maternal injections, final nymphal stage females were isolated and monitored daily for final molt. All females were injected with 15 μg of dsRNA on the third day following the final molt. Because we observed that egg laying could be reduced by the continued presence of two males, each female was housed separately with two males only for days one, two and five of a 10 day experiment.

Three different fragments of *Gb-oskar* were used as template for dsRNA synthesis (Fig. S3A): (1) *osk1*: a 742bp fragment starting 262 bp upstream of the first methionine and ending at position 480; (2) *osk2*: a 789 bp fragment from position 255-1044, and (3) *osk3*: a 503 bp fragment from position 638-1141. Results from these three fragments were consistent for all

phenotypic analyses. DsRNA was adjusted to a final concentration of 3 μg/μl (6.1 and 5.8 μM respectively) for fragments *osk1* and *osk2*, and 5 μg/μl for fragment *osk3* (15.1 μM). The *DsRed* negative control and *caudal* positive control dsRNAs have been described in [4] and were both used at the same final concentration as the corresponding *oskar* fragments used in that experiment (either 3 or 5 μg/μl).

Validating RNAi Knockdown

RNAi knockdown efficiency was estimated using both semi-quantitative RT-PCR and whole-mount antibody staining. For semi-quantitative RT-PCR (Fig. S3B), ovaries from maternal RNAi-injected females were dissected 10 days after maternal dsRNA injection, and stage 7-10 embryos laid by maternal RNAi-injected females, or resulting from zygotic RNAi injections, were dissected from 4-5 days after egg laying (AEL). All tissues were collected in Trizol (Invitrogen), and total RNA was isolated following manufacturer's protocols, followed by a 30 minute DNase treatment (Ambion) at 37°C to remove genomic DNA. Equal quantities of total RNA were used as template for first strand cDNA synthesis using SuperScript III (Invitrogen). *Gb-oskar* levels were estimated following 35 PCR cycles (98ºC for 3 minutes, 35 cycles of 98ºC for 30 seconds, 55ºC for 30 seconds, 72º C for 2 minutes 15 seconds, followed by a 10 minute final extension at 72ºC) and electrophoresis on a 1.0% agarose gel, compared to *Gb-beta-tubulin* to ensure equivalent amounts of template. Negative controls without reverse transcriptase were run in parallel and revealed no genomic DNA contamination. The *Gb-oskar* primers used (F: 5' TGGTAGTTCGAAGGGAACTTG-3'; R: 5'-CATCTTCCATTTGCCACAGA-3') amplify a band of 2,149 bp. The *Gb-beta-tubulin* primers used (F: 5'-TCAGACACCGTCGTTGAACC-3'; R: 5'-GATGGTTCAGGTCGCCGTAG-3') amplify a band of 157 bp.

Knockdown appeared to be less efficient using fragment *osk3* (Fig. S3B), but this fragment still produced CNS phenotypes consistent with those produced using fragment *osk1*.

RNAi efficiency was independently assayed by staining *osk* eRNAi and *DsRed* eRNAi embryos with the αGb-Oskar3501 antibody and imaging the embryos under identical conditions (Fig. S2F).

Scoring RNAi Phenotypes

To quantify egg laying, each injected female was individually housed with a dish of moist sand. Because we observed that *Gryllus* females typically only oviposit substantial numbers of eggs on alternate days, egg dishes were collected every 48 hours. Eggs were separated from sand using a 500 μm mesh under running tap water, and spread out in a monolayer in a 15cm petri dish. An image of the eggs was captured on a flatbed scanner and eggs were manually tallied using the ImageJ Cell Counter plug-in (Fig. S3C).

Ovarian morphology was assayed on ovaries of injected females 10 days after dsRNA injection. Wild type A-P patterning was assessed by the asymmetric localization of the oocyte nucleus in mid-stage oocytes [3]. We also tested for oogenesis phenotypes by looking for the presence of oocytes at all stages of development (Fig. S3D).

Embryonic morphology was visualized at stages 7-10 using both Nomarski optics and fluorescent nuclear staining (Fig. S3E). The presence of embryonic germ cells was assayed using in situ hybridization against *piwi* (not shown), as well as antibody staining for both Gb-Vasa and Gb-Piwi (Fig. 2G-H). The presence of functional ovarioles was also assayed in *osk* eRNAi embryos that were grown to adulthood.

Axonal scaffolds were visualized with anti-HRP immunostaining followed by confocal microscopy of the entire embryonic nervous system. Before scoring axonal defects, stage-matching of embryos was performed by comparison of morphogenetic progress in the thoracic appendages, antennae, abdominal segmentation and terminal cerci, rather than by developmental progression of the nervous system. Only embryos at stages 8.5-10 were used for this analysis, since formation of the global CNS axonal scaffold is complete by this time. Axonal patterning of *Gb-oskar* eRNAi embryos, *DsRed* eRNAi embryos, and uninjected embryos at comparable developmental stages were scored blind (embryos were grouped by matched developmental stages, but whether they were wild type, *DsRed* eRNAi or *Gb-oskar* eRNAi embryos was hidden) for consistent and symmetrical thickness and continuity of longitudinal connectives, timing/morphology of anterior commissure formation relative to central neuron mitoses, and timing/morphology of posterior commissure formation relative to anterior commissure formation. Two independent blind scoring rounds were performed and the results were consistent. After scoring was completed, the nature of the embryonic treatment was revealed, and data from embryos of the same treatment (uninjected, *DsRed* eRNAi or *Gb-oskar* eRNAi) were grouped for statistical analysis (Chi-squared test).

To test for defects in aCC/pCC neurons, we performed in situ hybridization on stage 9 embryos using a 528 bp probe against *Gryllus even-skipped.* Samples were scored blind for the absence of any of the four aCC/pCC neurons in each segment. Two independent knockdowns using two dsRNA fragments (fragments *osk1* and *osk3* described above) gave comparable results (5/11 and 5/18 embryos contained defective aCC/pCC neurons in the two experiments respectively). To reliably distinguish between aCC/pCC neurons and the nearby U/CQ neurons, we used several approaches. First, we noted that the U/CQ neurons are clearly distinguishable from aCC/pCC by their position in the dorsal-ventral axis and their relationship to the axonal scaffold. Specifically, aCC/pCC are the dorsal-most *eve*-positive cells while U/CQ are more ventral [see e.g. 3; their Figure 4a-h]. Second, aCC/pCC are reliably located in the corner where the longitudinal connectives meet the posterior commissure [see e.g. 4; their Figure 2d], and in the same focal plane. Third, in our analysis we examined optical sections through the entire dorso-ventral axis of every affected segment to ensure that apparently missing aCC/pCC cells were not visible in any other focal plane, and that U/CQ could be identified in more ventral focal planes.

Transgenic Constructs

To target HA-tagged Dm-Oskar or Gb-Oskar to the *D. melanogaster* oocyte anterior, we cloned Gb-Oskar, Dm-Losk(M1L):Gb-Oskar, or Dm-Osk-bcd3'UTR [5] into pValium22 [6], which contains attB sites for PhiC31-based targeted integration and is optimized for expression in the female germ line. We used a previously described bcd3'UTR that has a putative NRE replaced by a 10bp linker to prevent potential transcript clearing by *nanos* [5, 7]. Cloning was performed using the circular polymerase extension cloning method [8] with primers containing an N-terminal HA-tag (pValium22 was amplified with primers F: 5'-AGAACTAGAGCCGCG-3', R: 5'GCCCGAGCTTAAGACT-3'; Dm-Osk-bcd3'UTR was amplified with primers F: 5'-GCCAGTCTTAAGCTCGGGCATG
TACCCATACGATGTTCCGGATTACGCTGCCGCAGTCACAAGT-3' and R: 5'-CAATTCCGCGGCTCTAGTTCTGGATCCACCCGAGTA-3'; Gb-Oskar was amplified with primers F: 5'-GCCAGTCTTAAGCTCGGGCATG
TACCCATACGATGTTCCGGATTACGCTAGTTGGACTGAGGTT-3' and R: 5'-

CCTCTCATCCAGGCTCGAGCGCCGGCGTCAATGTGTGTTTTC-3'; to amplify the bcd3'UTR for fusion with Gb-Oskar, primers F: 5'-CTCGAGCCTGGATGA-3' and R: 5'-CAATTCCGCGGCTCTAGTTCTGGATCCACCCGAGTA-3' were used). The transgenes for GbOsk:bcd3'UTR and DmOsk:bcd3'UTR were inserted into the attp40 site on 2L, and the DmLosk(M1L):GbOsk:bcd3'UTR transgene was inserted into the attp2 site on 3L [9] both of which show high levels of specific expression. Injection to create transgenic flies was carried out by Genetic Services, Inc. (Cambridge, MA). Transgenic progeny were identified and maintained using standard genetic crosses.

Drosophila Stocks

The maternal driver line *w^{*}; P{w^{+mC}=matalpha4-GAL-VP16}V2H* was obtained from the Bloomington *Drosophila* Stock Center (stock number 7062). *y v; Sco/CyO* and *y sc v ; Dr e/TM3,Sb* were obtained from the Perrimon lab (Harvard University).

Imaging and Image Analysis

Images were captured with AxioVision v.4.8 driving a Zeiss Stereo Lumar equipped with an AxioCam MRc camera, or a Zeiss Axio Imager equipped with an AxioCam MRm camera, using epifluorescence either with or without an Apotome. Confocal microscopy was performed with a Zeiss LSM 710 confocal, using comparable gain, offset, and averaging parameters for all samples. Image analyses were performed with AxioVision v.4.8, Zen 2009 (Zeiss), and figures were assembled in Photoshop CS4 or Illustrator CS4 (Adobe). For the confocal images shown in Fig. 2 (G-N), a maximum-intensity projection of the antibody staining was superimposed over a single z-plane of the nuclear counterstain for visual clarity.

Author Contributions: BE-C and CGE designed research, analysed data and wrote the paper; experiments were carried out by JRS (recombinant Gb-Oskar purification), EES (cloning *Gb-vasa* and *Gb-piwi*), CGE (axonal scaffold phenotypic analysis) and BE-C (all other experiments); CGE obtained funding for the research.

Supplemental References

1. Anantharaman, V., Zhang, D., and Aravind, L. (2010). OST-HTH: a novel predicted RNA-binding domain. Biology Direct *5*, 13.

2. Callebaut, I., and Mornon, J.-P. (2010). LOTUS, a new domain associated with small RNA pathways in the germline. Bioinformatics *26*, 1140-1144.

3. Lynch, J.A., Peel, A.D., Drechsler, A., Averof, M., and Roth, S. (2010). EGF signaling and the origin of axial polarity among the insects. Curr. Biol. *20*, 1042-1047.

4. Kainz, F., Ewen-Campen, B., Akam, M., and Extavour, C.G. (2011). Delta/Notch signalling is not required for segment generation in the basally branching insect *Gryllus bimaculatus*. Development *138*, 5015-5026.

5. Tanaka, T., and Nakamura, A. (2008). The endocytic pathway acts downstream of Oskar in Drosophila germ plasm assembly. Development (Cambridge, England) *135*, 1107-1117.

6. Ni, J.-Q., Zhou, R., Czech, B., Liu, L.-P., Holderbaum, L., Yang-Zhou, D., Shim, H.-S., Tao, R., Handler, D., Karpowicz, P., et al. (2011). A genome-scale shRNA resource for transgenic RNAi in Drosophila. Nature Chemical Biology *8*, 405-407.

7. Ephrussi, A., and Lehmann, R. (1992). Induction of germ cell formation by *oskar*. Nature *358*, 387-392.

8. Quan, J., and Tian, J. (2011). Circular polymerase extension cloning for high-throughput cloning of complex and combinatorial DNA libraries. Nature protocols *6*, 242-251.

9. Markstein, M., Pitsouli, C., Villalta, C., Celniker, S.E., and Perrimon, N. (2008). Exploiting position effects and the gypsy retrovirus insulator to engineer precisely expressed transgenes. Nat. Genet. *40*, 476-483.